Regional carbon predictions in a temperate forest using satellite lidar

Article (Accepted Version)

Regional Carbon Predictions in a Temperate Forest using Satellite Lidar

Alexander S. Antonarakis, Alejandro Guizar Coutiño

***Abstract*— Large uncertainties in terrestrial carbon stocks and sequestration predictions result from insufficient regional data characterizing forest structure. This study uses satellite waveform lidar from ICESat to estimate regional forest structure in central New England, where each lidar waveform estimates fine-scale forest heterogeneity. ICESat is a global sampling satellite, but does not provide wall-to-wall coverage. Comprehensive, wall-to-wall ecosystem state characterization is achieved through spatial extrapolation using the random forest machine learning algorithm. This forest description allows for effective initialization of individual-based terrestrial biosphere models making regional carbon flux predictions. Within 42/43.5 N and 73/71.5W, above-ground carbon was estimated at 92.47 TgC or 45.66 MgC ha^{-1}, and net carbon fluxes were estimated at 4.27 TgC yr^{-1} or 2.11 MgC ha^{-1} yr^{-1}. This carbon sequestration potential was valued at 47% of fossil fuel emissions in eight central New England counties. In preparation for new lidar and hyperspectral satellites, linking satellite data and terrestrial biosphere models are crucial in improving estimates of carbon sequestration potential counteracting anthropogenic sources of carbon.**

***Index Terms*— Ecosystem Modelling, Lidar, Regional Carbon Fluxes, Temperate Forest**

I. Introduction

THE largest remaining uncertainties in the Earth's carbon budget are in its terrestrial components [1]. Reducing this uncertainty will result from more accurate methods determining the current state of terrestrial ecosystems at a variety of scales essential in monitoring and managing terrestrial carbon stocks [2]. Reducing the uncertainty will also depend on improving predictions of ecosystem changes in response to climate change using ecosystem models [3,4,5]. One key to improving model prognostic abilities is to reduce the initialization error: errors arising from the description of the ecosystem's state at the beginning of the prediction period. By reducing this error (as well as the climate forcing error) we can obtain better understanding of model process/parameterization errors which will further improve carbon cycle predictions. Information on current carbon stocks has traditionally come from ground-based inventories that provide detailed information on the composition and structure of the plant canopy, but are spatially limited, expensive to establish, or are scarcely-existent in many parts of the world. In contrast, remote sensing offers the promise of large scale, spatially-consistent data on key aspects of current ecosystem state.

Remote sensing estimates of ecosystem structure have been derived using active remote sensing techniques such as lidar and radar [6,7], defining metrics such as forest canopy height [8,9] and aboveground biomass (10,11,12). Estimating ecosystem composition, in the last few decades, has taken the form of land cover products based on multi-spectral imagery, such as MODIS International Geosphere-Biosphere Program (IGBP) scheme [13] or the National Land Cover Dataset [14], and more recently through imaging spectrometry [15,16,17]. Remote sensing products have been used to test, validate and constrain output from terrestrial biosphere models. Vegetation structure from airborne radar has been used to initialize terrestrial biosphere models as diagnostic tools of land cover change [12,18]. Airborne lidar-derived structure has been used to parameterize canopy photosynthesis models (e.g. 19,20,21), providing evidence of impact on carbon flux estimates. Recent studies [22,23,24] have used lidar heights and biomass to improve carbon fluxes at temperate and tropical forests, using the Ecosystem Demography model (ED2 [25,26]).

A recent analysis [26] showed that individual-based terrestrial biosphere models (e.g. ED2 model) that incorporate *fine-scale* heterogeneity in ecosystem structure and composition can be better constrained than conventional big-leaf models, resulting in more accurate predictions of spatial variability in terrestrial carbon fluxes. Levine *et al*. [27] also showed that heterogeneity in fine-scale ecosystem structure and composition strongly influences their resilience and response to climatological perturbations. A recent study at a temperate forest in central Massachusetts, [28] assessed the potential of combining *airborne* lidar and hyperspectral remote sensing data to provide information on *fine-scale* forest ecosystem structure and composition necessary to correctly initialize the above-ground ecosystem state in the ED2 biosphere model, resulting in improved carbon flux predictions (reduced net carbon flux errors by 50% compared to potential vegetation runs). The fine-scale size structure in [28] was derived using the full vertical foliage profile from airborne lidar, and plant functional type composition was derived using spectral mixture analysis applied to hyperspectral imagery.

In this study, we demonstrate the regional-scale applicability of the Antonarakis *et al*. [28] methodology using *satellite* lidar from ICESat, rather than *airborne* techniques, to provide measurements of regional ecosystem structure in central New England and terrestrial biosphere model predictions of carbon fluxes. Landmark studies by Saatchi et al. [10] and Baccini et al. [11] have used ICESat to define above-ground biomass

This paragraph of the first footnote will contain the date on which you submitted your paper for review.

This work was supported by the Sussex Research Development Fund under Grant # 4290.

A.S. Antonarakis is with the Department of Geography, Sussex University, Chichester 1, Falmer, Brighton, BN1 9QJ, Email: a.antonarakis@sussex.ac.uk; Telephone: +44 (0)1273-87-3490.

A. Guizar Coutiño is with the Luc Hoffman Institute, WWF International, 1196 Gland, Switzerland. Email: aguizar@wwfint.org.

(ABG). These studies defined AGB by using regression techniques based on related satellite lidar-height and return energy metrics to field derived AGB, and spatially extrapolating using machine learning algorithms. These height metrics included HOME (height-of-median-energy), H100 (top of the canopy), H10 to H90 (10% to 90% of height above ground), or Lorey's height (basal-area weighted height). This study will use the full satellite lidar waveform to determine fine-scale heterogeneity in ecosystem state per satellite footprint. ICESat is a global technique, but does not provide wall-to-wall coverage. Comprehensive, wall-to-wall ecosystem state ready for initialization using the ED2 model is achieved through spatial extrapolation using the random forest machine learning algorithm. Testing this methodology estimating regional carbon fluxes is now crucial in preparation for newer, more spatially consistent satellite waveform lidar from Global Ecosystem Dynamics Investigation Lidar (GEDI), as well as a hyperspectral satellite (Hyperspectral InfraRed Imager).

II. Methodolgy

In this study, individual GLAS satellite lidar shots within a defined region in New England are first chosen. Second, quality maintenance is performed removing shots that are not ground reflectances or have a limited vertical profile. Third, estimates of forest composition are determined using high resolution regional land cover products and national forest inventories. Fourth, size class distributions encompassing tree sizes, density and plant functional types for each GLAS waveform are derived using the method set out in [28]. Fifth, the Random Forest algorithm is used to extrapolate forest structure to the region where no GLAS data exists, using a number of edaphic, climatic and land cover conditions. Sixth, the number of trees per size class and plant functional groups are attributed to each pixel in the extrapolated region. Finally, the ED2 model is used to predict short-term carbon fluxes by initializing simulations using regional forest structure and composition. Details of the methodology are provided below.

A. ED2 Biosphere Model

The ED2 (Ecosystem Demography) Model is an integrated terrestrial biosphere model calculating the exchange of carbon, water, and energy, incorporating hydrology, land-surface biophysics, vegetation dynamics, and soil carbon and nitrogen biogeochemistry [25], [26]. ED2 utilises a set of size- and age-structured partial differential equations that track the changing structure and composition of the plant canopy. The model is first divided into grid cells that experience the same meteorological forcing. Each grid cell is subdivided into a number of horizontal tiles representing areas of forest that share a similar vegetation canopy structure and disturbance history. Finally, the ecosystem state within each tile is described by the density of individual trees of different sizes, for a series of plant functional types. Each plant functional type differs in terms of its leaf physiology that results in different rates of growth and mortality and sensitivity to environmental conditions.

B. Study Region and Lidar Preprocessing

The study area is a temperate forest region in central New England, USA, with upper left and lower right boundary coordinates of 43.5 N 73.0 W and 42.0 N 71.5 W. This region

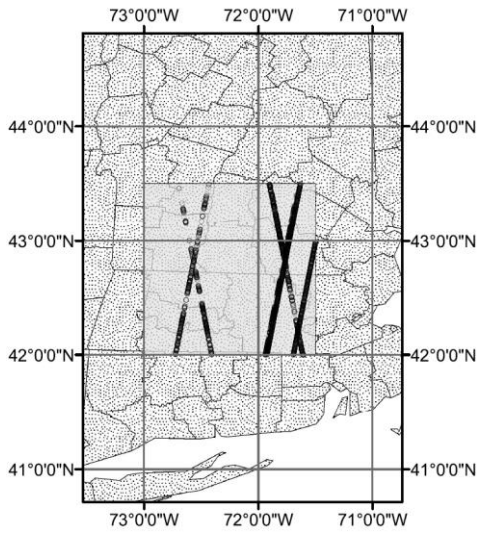

Fig. 1. Location of the study region in central New England with locations of summer IceSAT transect lines with final pulse locations. Raw waveforms were available only for south-west to north-eastern lines.

was chosen as the ED2 model has been calibrated and validated [26], and the derivation of forest structure from waveform lidar has been developed/calibrated here [28]. Forests in this region are northern hardwoods and transitional hardwood and conifer forests dominated by oaks, maples, pines and hemlocks. For this region, five plant functional types (PFTs) have been parameterised in ED2 [26] as early-successional conifers (e.g. *Pinus resinosa* and *Pinus strobus)*, late-successional conifers (e.g. *Tsuga canadensis*, *Picea rubens*), early-successional hardwoods (e.g. *Betula ssp*), mid-successional hardwoods (e.g. *Quercus ssp.*, *Acer rubrum*, *Fraxinus americana*), and late-successional hardwoods (*Fagus ssp, Acer saccharum*).

LiDAR waveform data were obtained by the Geoscience Laser Altimeter System (GLAS) on-board NASA's ICESat (Ice, Cloud, and land Elevation Satellite) [29]. The GLAS laser transmits pulses at 1064 nm with a footprint size of around 70 m spaced around 172 m meters apart. Within the study region, GLA01 and GLA14 data were extracted only from June to September 2004-2006 (maximum leaf-on conditions). GLA01 contains the raw waveform, while GLA14 is the altimetry product providing information on the beginning and end of each pulse, the ground return location, and also provides the locations, amplitude and standard deviation of up to 6 Gaussian curves which when added together make up the modelling waveform (see [30]). In this study both modelled and raw waveforms were extracted and cut from the signal beginning (tree top) to the signal end, incorporating the position of the ground return and the full foliage return of the canopy.

To remove unreliable GLAS shots, the data was screened based on a number of criteria; a) waveforms had to be more than two peaks; b) the amount of baseline noise had to be below two times the maximum amplitude; c) GLAS-derived elevation differed from SRTM elevation by less than 25m; d) the ground slope of each pulse had to be less than 10^{o} [31] using the National Elevation Dataset (NED). This finally resulted in around 3100 modelled and 2000 raw waveform pulses. The locations of the IceSAT transect lines with final pulses, and the study region are shown in Fig. 1.

C. Forest Composition and Structure

Determining sub-pixel forest structure from GLAS pulses follows the method developed in [28], and is described here. This method relates full waveform lidar with knowledge of PFT-dependent specific leaf area and leaf biomass. In [28] PFTs were derived using airborne imaging spectroscopy. Regional spatially consistent imaging spectroscopy is not yet available, so a different approach was used to determine regional forest composition. The 30 m 2006 National Land Cover Database (NLCD) was used to extract the hardwood, conifer, and mix woodland fraction averaged within each pulse. Subsequently, USDA Forest Inventory and Analysis (FIA) plots were used to attribute PFTs to each NLCD forest class. The FIA plots provide tree sizes and species for around 500 plots in the study region. Basal area was determined for each FIA plot where species were converted to one of the five temperate ED2 PFTs (see section 2.2 for PFT descriptions). NLCD Conifer dominated stands (>75% conifers) were attributed PFTs from conifer dominant FIA plots of 60/27/3/9/1%, hardwood dominated stands (>75%) were attributed PFTs of 4/4/12/58/22%, and Mixed stands 26/21/9/37/7% for early, late successional conifers, and early, mid and late successional hardwoods respectively. This resulted in relative PFT abundance per lidar pulse, and per pixel of the study region. In this step (section 2.3), FIA data were only used to attribute PFT abundances to NLCD forest classes, deriving a regional forest composition product.

Estimating forest structure from the GLAS waveform relies not only on PFT information per pulse (as above), but on estimating the vertical foliage profile of each pulse. Leaf Area Index profiles of a lidar pulse of PFT *i*, at location *x*, and height bin h ($LAI^i(h,x)$) were estimated using the lidar gap fraction ($\mathrm{P}(h,x)$) determined from [32] and the clumping factor (γ).

$$LAI^i(h,x) = q^i(x)\left[\frac{d}{dh}\left(\frac{-2\ln(P(h,x))}{\gamma^i}\right)\right] \quad (1)$$

Where $q^i(x)$ is the relative abundance of PFT i at location *x*, estimated from NLCD/FIA. The clumping factor for hardwood PFTs was 0.93 and for conifers was 0.74 [33-34]. The LAI profiles calculated from Equation (1) are then used to estimate the density profile of each pulse $n^i(h,x)$:

$$n^i(h,x) = \frac{LAI^i(h,x)}{SLA^i * B^i_{leaf}(h)} \quad (2)$$

Where SLA^i and B^i_{leaf} are the specific leaf area and leaf biomass of PFT *i*. The PFT-dependent SLA and leaf biomass values and allometries are the same specified in the ED2 model, and can be found in [28]. To initialize the ED2 model, the tree density with height ($n^i(h,x)$) of each PFT i (Equation 2) needs to be translated into a corresponding diameter size distribution ($n^i(z,x)$) using the height-to-diameter function $DBH = 10\text{^}(b_1 * h + b_2)$ used in ED2, where the coefficients (b_1/b_2) for each of the PFTs were defined using FIA within the study 1.5x1.5° region (see [28]). The final product from this method is a distribution of tree sizes and plant functional types, *for each individual pulse*. Basal area per pulse can therefore be calculated the same as using forest inventory plots; with knowledge of all tree diameters within a plot area. This method has been validated in [28] over 88 plots at Harvard Forest, Massachusetts, using airborne lidar waveforms, with root-mean-square-errors (RMSEs) of 10 m^2 ha^{-1}. Resulting basal area calculated from *modelled* and *raw* satellite waveform in this study, are compared to ground observations under the GLAS footprints. Twenty-two ground plots measuring tree species and trunk circumference greater than 10 cm in 800m^2 plots located in the center of a GLAS footprint were collected in May 2015. These 22 plots were spread out over 60 km in a North-South transect, from Worcester, Massachusetts, to Peterborough, New Hampshire. As these plots were measured 9-10 years after the ICESat data, a mean and standard deviation change was applied using the aforementioned ground plots at Harvard Forest, resulting in yearly basal area change of 0.34 m^2 ha^{-1} yr^{-1} with a standard deviation of 0.33 m^2 ha^{-1} yr^{-1}.

D. Spatial Extrapolation

Extending satellite lidar-derived size class distributions to the 1.5x1.5° study region requires wall-to-wall edaphic, climate and land cover layers and a spatial extrapolation algorithm. In this study the Random Forest Machine Learning algorithm [35] was used. Wall-to-wall datasets included the NLCD percent canopy cover and hardwood fraction; elevation, slope and aspect from the 1 arc-second US National Elevation Dataset; percentage sand and clay, saturated hydraulic conductivity (μm s^{-1}) and available water capacity (cm_{water}/cm_{soil}) from the Soil Survey Geographic database (SSURGO; 1 arc-second); and yearly precipitation, average monthly minimum and maximum temperature, and vapour pressure from 1km resolution Daymet [36] averaged over 1990-2010. These 13 layers were produced at the scale of the GLAS footprint and at 1km resolution for the 1.5x1.5° region. For the GLAS footprint only, more representative canopy cover was derived using the lidar gap profile as in [32]. The response variable for the Random Forest algorithm was the basal area derived from GLAS modelled waveform, not the raw waveform. The modelled waveform covered a larger spatial extent and the differences in derived basal area between modelled and raw products were small [less than a RMSE of 2.5 m^2 ha^{-1} (see Fig. S1) and nearly equal when compared to the ground plots (results stated in section 3)].

Random Forest was trained and tested for an 80/20% subset of the 3100 GLAS shots, using 1000 random trees. Consequently, regional 1 km resolution basal area was predicted. Yet, to initialize forest structure and composition in each pixel using ED2, there is need for the full description of tree size classes and PFTs, not just the basal area. The use of 1000 random trees and 13 predictor variables meant that basal area predictions using Random Forest at each 1km pixel could comprise dozens of GLAS datapoints used in the fitting exercise. Therefore, for each pixel in the 1.5x1.5° region, single GLAS pulses identified with a resulting total basal area (section 2.3) and NLCD hardwood fraction RMSE within 0.3 m^2 ha^{-1} and 10% respectively were *matched* with Random Forest estimated basal area per pixel. Each individual GLAS pulse, using the method set out in [24] and in section 2.3, results in a full distribution of tree sizes and plant functional types. When resulting sub-pixel structure and composition derived for individual GLAS lidar pulses are attributed to each 1km pixel in the 1.5x1.5° region, the actual RMSE of the matching exercise, ends up less than 0.13 m^2 ha^{-1} compared to the

Random Forest predicted basal area and 5% to the NLCD hardwood fraction.

Results from the Random Forest were compared to ground plots, to the 20% testing data sample, and thirdly to available FIA national forest inventories. The FIA plots do not provide exact coordinates, but locations to within 1km. Yet, certain edaphic and land cover layers are given for each plot including elevation, slope, aspect, % hardwood, and canopy cover. The remaining climate, soil texture, and soil water layers were averages of the surrounding 1km. Using these layers and FIA data, Random Forest was run to produce estimates of basal area.

E. Regional Carbon Fluxes

ED2 simulations were conducted for the full region outlined in Fig. 1 to demonstrate and determine carbon fluxes after initializing regionally forest structure and composition. Simulations were done from 2004-2008 where each lidar pulse was a tile, and cohorts were the waveform-derived size class distributions. Regional climate forcing encompassing hourly over-canopy air temperature, downward shortwave and longwave radiation, precipitation, specific humidity, wind velocities, and surface air pressure, were obtained from the North American Land Data Assimilation Version 2 (NLDAS-2) with a spatial resolution of 1/8° [37]. Soil depth to bedrock and soil carbon were obtained from STATSGO (1km), and soil texture from the SSURGO database (1 arc-second). Hardwood phenology was prescribed using MODIS, based on fitting logistic functions to dates for green-up, maturity, senescence, and dormancy of leaves [26].

Uncertainty estimates of the forest structure and carbon fluxes predicted at the 1.5x1.5° study region were also included in this analysis. The uncertainty in basal area was determined from the RMSE resulting from comparisons between Random Forest predicted basal area and combined ground plots, FIA plots and the testing GLAS dataset (Fig 2). RMSEs and percent uncertainty were binned and averaged at 5 m^2 ha^{-1} intervals and then applied to each pixel in the 1.5x1.5° region. The uncertainty at each 1km pixel was propagated and initialized using the ED2 model. Uncertainty of carbon stocks and fluxes at the level of eight New England counties ranging from around 1400-4000 km^2 were produced according to Saatchi et al. [10] and Rodríguez-Veiga et al. [38], increasing the sample area and propagating the error at the 1km pixel level to the regional level.

III. RESULTS

A. Forest Structure from Satellite Lidar

Basal area calculated from modelled GLAS resulted in an RMSE of 9.4 m^2 ha^{-1} (9.3-10 m^2 ha^{-1} incorporating the standard deviation of plot basal area change within 9-10 years) and R^2 of 64% compared to ground-based basal area (Fig. 2a closed circles). Without incorporating change into these plots, the resulting RMSE is 9.58 m^2 ha^{-1}. Forest composition defined using NLCD and FIA resulted in abundance errors of 19% with ranges of 11-28% for the five PFTs. Forest structure was also derived using the raw waveform resulting in basal areas differences of only 2.5 m^2 ha^{-1} compared to modelled waveforms (see Fig. S1), and similar errors compared to the observations (RMSE of 9.19 m^2/ha and R^2 of 63%). Examples of model and raw lidar waveforms, estimated and observed size class distributions are presented in the supplement (Fig. S2). Random Forest-predicted basal area was tested on 20% of the modelled GLAS samples resulting in basal areas with an RMSE of 9.85 m^2 ha^{-1} and an R^2 of 75% (Fig. 2b). Furthermore, Random Forest-predicted basal area was tested on the 22 observation plots (not included in training), resulting in errors of 10.42 m^2 ha^{-1} and R^2 of 43% (Fig. 2a). Finally, Random Forest-predicted basal areas were compared to 520 FIA plots, resulting in errors of 10.58 m^2 ha^{-1} and R^2 of 34% (Fig. 2c).

B. Regional Carbon Estimates

Regional estimates of forest structure, composition, and carbon fluxes are presented in Fig. 3. The basal area (Fig. 3i) shows areas ranging from sparse to densely forested regions of up to 50 m^2 ha^{-1}. There is a distinction between dense forested areas in the center, north and the northwest of the region, and sparser forested areas in the more populated southern regions of the Connecticut River valley, Eastern Massachusetts and New Hampshire. AGB shown in Fig. 3ii uses ED2 model allometry to determine current carbon stocks resulting in 92.47 TgC or 45.66 MgC ha^{-1}. Fig. 3iii, iv show basal area of hardwoods and conifers using NLCD and FIA described in this study. In these figures, there is a distinction in forested ecoregions with the south and west of the region dominated by hardwoods, and center and north containing mixed conifers and hardwoods.

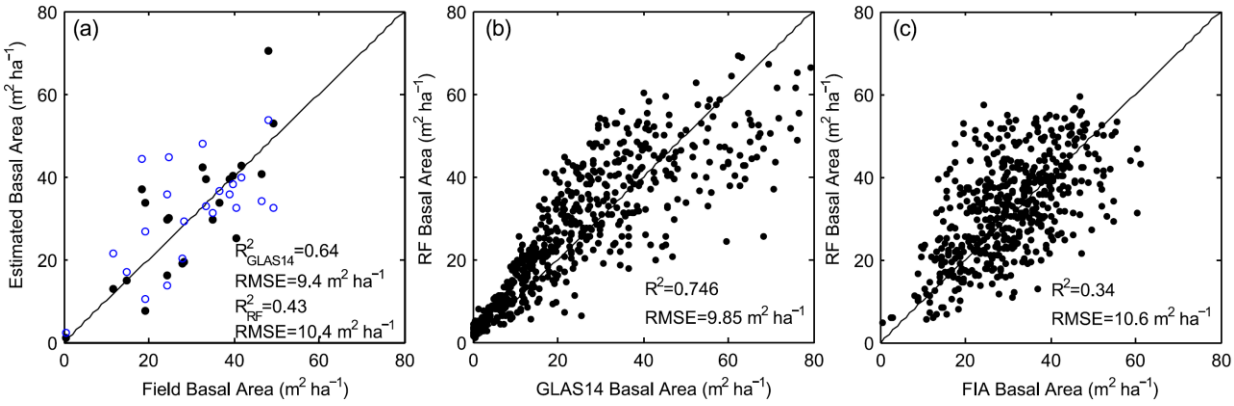

Fig 2. Comparisons between basal area derived from satellite lidar modelled waveform and from 22 field observations (panel a: closed circles), and comparisons between Random Forest predicted basal area and field observations (panel a: open circles). Random Forest predicted basal area compared to the testing set of 610 satellite lidar-derived basal area is shown in panel b). Random Forest predicted basal area compared to the 520 Forest Inventory and Analysis (FIA) calculated basal area is shown in panel c).

ED2 was run initializing forest structure and composition estimated in this study, resulting in gross primary productivity (GPP; Fig. 3v) and net ecosystem productivity (NEP: Fig. 3vi) estimates. This resulted in yearly NEP of 4.27 TgC yr^{-1} or 2.11 MgC ha^{-1} yr^{-1}, and GPP of 29.29 TgC yr^{-1}. Errors associated with forest structure derived in this study, and its propagation through ED2 predicted carbon fluxes are shown in Fig. 4. Uncertainty in basal area ranged from 20-55% with an average uncertainty of 37% (Fig. 4a). Higher uncertainty was found in pixels with lower basal areas, e.g. < 25 m^2 ha^{-1}. At pixel level, this corresponded to an average AGB error (Fig. 4b) of 20 (*s.d.* 8.1) MgC ha^{-1}. The predicted NEP error ranged up to 1.6 MgC ha^{-1} yr^{-1} and averaged 0.6 (*s.d.* 0.33) MgC ha^{-1} yr^{-1} or 28%.

County level basal area, carbon stocks (AGB) and carbon sequestration (NEP) is also offered in Table 1. Fossil fuel emissions at the level of the eight counties in Massachusetts, Vermont, and New Hampshire are also provided in Table 1, and were obtained from the Vulcan Project running from 1999-2008 [39]. For these eight counties the NEP is estimated at 3.45 ± 0.026 TgC yr^{-1} with fossil fuel emissions given as 7.36 TgC yr^{-1}. Pixel-level uncertainty within the eight counties ranged from 0.38-0.68 MgC ha^{-1} yr^{-1} or 16-37%.

IV. Discussion

This study has used satellite waveform lidar and other edaphic, land cover, and climate layers to estimate *fine-scale* heterogeneity in forest structure and composition at the regional scale. This description of the above-ground ecosystem allows for direct and effective initialization using individual-based terrestrial biosphere models to make regional predictions of ecosystem carbon fluxes. Over a region in central New England, total above-ground carbon stocks were estimated at 92.47± 0.3 TgC or 45.66 ± 20 MgC ha^{-1}, and net yearly carbon fluxes were estimated at 4.27± 0.01 TgC yr^{-1} or 2.11± 0.6 MgC ha^{-1} yr^{-1}. This carbon sequestration potential was valued at around 25% of the total fossil fuel emissions in four central Massachusetts counties, but similar to or greater in four largely rural Vermont and New Hampshire counties, resulting in a total sequestration potential of the eight countries at 47% of fossil fuel emissions. Testing and determining regional scale carbon stocks and fluxes linking satellite data and terrestrial biosphere models is crucial in preparation for new satellite waveform lidar (GEDI) and high resolution imaging spectroscopy (HyspIRI). This will bind regional to potentially global carbon-fluxes with remote sensing, reducing this uncertainty source in climate

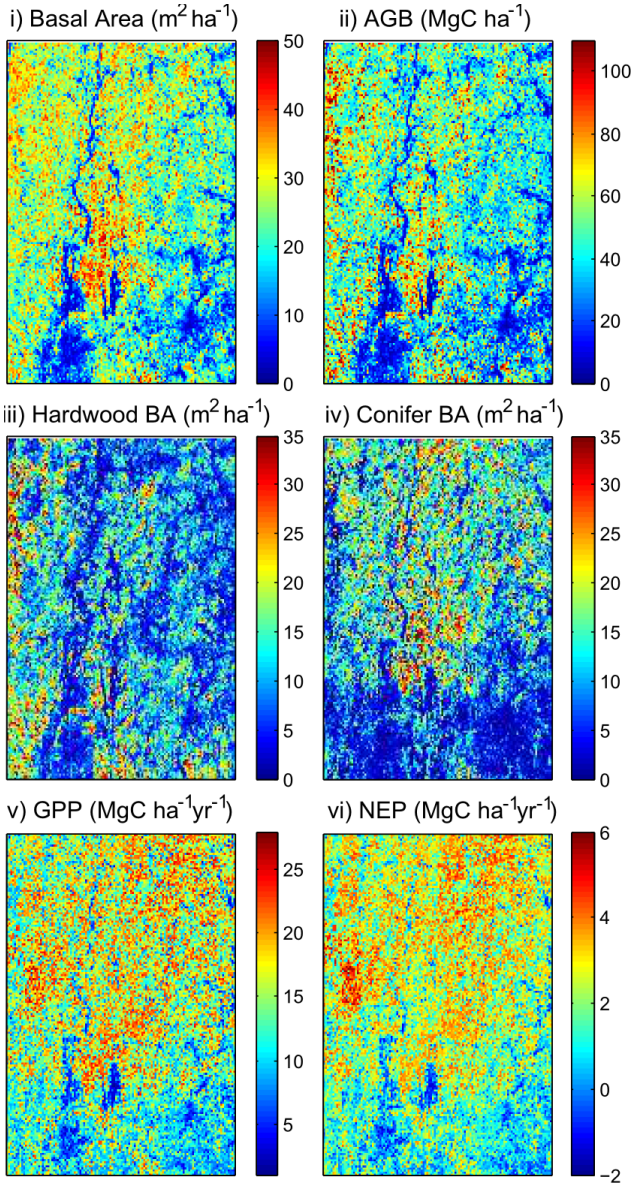

Fig. 3. Regional Estimates of Forest Structure, Composition, and Carbon Fluxes for the 166 x 122 km region (1km resolution). Panel i) illustrates the basal area and Panel ii) shows AGB using ED2 model allometry. Panels iii) and iv) show the basal area of hardwoods and conifers. Panels v) and vi) illustrate yearly average short-term (2004-2008) gross primary (GPP) and net ecosystem productivity (NEP) resulting from ED2 runs initialized with the forest structure and composition derived in this study.

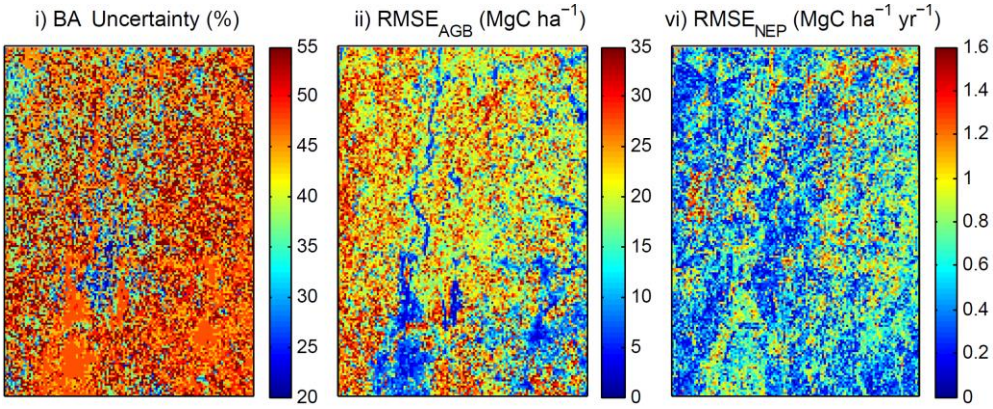

Fig 4. The uncertainty of the forest structure and carbon stocks and flux estimates for the 166 x 122 km region. Panel i) shows the uncertainty given in percent error derived by comparing Random Forest predictions of basal area to testing and ground observation datasets. Panel ii) shows the uncertainty in Panel i) affecting the error in above-ground-biomass. Panel iii) shows the uncertainty in Panel i) propagated through the ED2 model, resulting in an error in net ecosystem productivity (NEP) predictions.

models, and improve our ability to understand the magnitude of carbon sequestration potential.

TABLE 1
COUNTY LEVEL CARBON STOCKS AND NEP (2004-2008)

State	County	BA (m^2 ha^{-1})	AGB (MgC ha^{-1})	AGBtotal (TgC)	NEP (MgC ha^{-1} yr^{-1})	NEPtotal (TgC yr^{-1})	Fossil Fuel Emissions (TgC yr^{-1})
MA	Worcester	19.17 ± 8.7	38.83 ± 17.8	15.81 ± 0.13	1.55 ± 0.48	0.63 ± 0.004	3.15
MA	Hampshire	20.81 ± 9.5	43.95 ± 19.9	6.11 ± 0.08	1.54 ± 0.45	0.21 ± 0.003	0.45
MA	Hampden	19.07 ± 8.7	41.77 ± 18.9	6.95 ± 0.09	1.12 ± 0.41	0.19 ± 0.003	1.79
MA	Franklin	25.83 ± 10.3	50.82 ± 20.3	9.56 ± 0.10	2.09 ± 0.38	0.39 ± 0.003	0.40
VT	Windham	26.73 ± 11.4	53.46 ± 22.6	11.08 ± 0.11	2.84 ± 0.53	0.59 ± 0.003	0.22
NH	Cheshire	26.01 ± 10.9	49.77 ± 20.9	9.46 ± 0.10	2.60 ± 0.45	0.49 ± 0.003	0.23
NH	Hillsborough*	22.20 ± 10.5	41.83 ± 19.8	9.68 ± 0.11	2.34 ± 0.63	0.54 ± 0.004	0.97
NH	Sullivan*	26.41 ± 11	49.28 ± 20.6	6.94 ± 0.09	2.83 ± 0.44	0.40 ± 0.003	0.15

*County level fossil fuel emissions were taken from the Vulcan Project (Gurney et al. 2009). *Carbon estimates for Hillsborough & Sullivan, NH were averaged over 84 & 83% of the county areas.*

Full waveform GLAS data fused with information on canopy composition from NLCD and FIA, has estimated forest structure with sub-pixel heterogeneity within each individual pulse (e.g. see Fig. S2) using the method introduced in Antonarakis et al. [28]. Antonarakis et al. [28] used airborne waveform lidar and imaging spectroscopy data to derived fine-scale forest structure and composition within a 4 km^2 area, and was validated over 88 plots at Harvard Forest, central Massachusetts with an RMSE of 10 m^2 ha^{-1}. Using available satellite lidar, this present study was able to estimate forest structure to a similar error of 9.4 m^2 ha^{-1} over 22 plots (Fig. 2a). Uniquely, this method does not require calibration with ground plots, but requires estimates of specific leaf area and leaf biomass per PFT, identified in the ED2 model, where a PFT can have similar leaf parameters in a biome or ecosystem. Spatially extrapolating estimates of GLAS-derived forest structure using Random Forest (Fig. 2b), resulted in a testing data error of 9.85 m^2 ha^{-1} (with 37% uncertainty), and an error of 10.58 m^2 ha^{-1} (with 35% uncertainty) when validating with 520 available FIA plots in the region (Fig. 2c). The FIA dataset in itself introduces error due to a) no explicitly available soil texture and moisture parameters, and b) the use of the ocular method to determine canopy cover [40]. The ocular method is a visual estimate of canopy cover using a sample of predefined images and is easy to implement, but is likely to ignore subplot boundaries, is difficult to assess medium canopy cover areas, and is based on the judgement of different estimators [41].

Current forest ecosystem state, estimated using satellite waveform lidar, NLCD and other edaphic, land cover, and climate layers were applied to the 1.5x1.5° region in central New England (Fig. 3) using Random Forest. Uncertainty in estimates of forest structure were propagated through the ED2 model predicting carbon fluxes. Pixel-based estimates of uncertainty of 20-55% (Fig. 4a) and averaging around 37% is similar to the uncertainty stated in Saatchi et al. [10] with values of 31% (6-53%) for pantropic AGB estimates. As in [10], uncertainty was constrained at larger spatial scales to just over 1% for AGB (92.47± 0.3 TgC) by propagating the error at the pixel-level to the region. Propagating the pixel-level error in ED2 NEP estimates (Fig. 4c) resulted in pixel errors of 28%, and regional errors of 1%.

The ability to use satellite waveform lidar, both using IceSAT and future satellites, to initialize terrestrial biosphere model simulations is important because these instruments can provide the actual ecosystem state rather than needing detailed ground observations, or working with potential vegetation from long-term equilibrium simulations. Reduction in uncertainty in deriving forest structure will come from higher resolution and more spatially consistent satellite lidar such as the future GEDI mission. Beyond GEDI, other future satellites will detect vertical canopy profiles, including IceSAT-2, BIOMASS (multi-baseline interferometric P-band radar), and NISAR (interferometric L-band). There may be the potential to use Fourier transform approaches to obtain vertical profiles [42], or develop *a priori* foliage distribution functions and apply them to a set of forests structural or functional types.

Forest composition in this study was estimated by applying abundances of five temperate PFTs from national forest inventories to broad forest land cover classes. Future satellite imaging spectroscopy (HyspIRI; EnMAP) will provide an effective way to derive PFT abundances for large contiguous areas, reducing forest composition errors, and subsequently improve carbon flux predictions. Furthermore, these future lidar, radar, and imaging spectroscopy satellites will provide other important regional information such as tree height, biomass, but also canopy biochemistry from imaging spectroscopy, which may help refine spatial extrapolation methods. Finally, the carbon stocks and sequestration potential for the simulation period are provided. Improvements to these simulations on top of reducing errors in estimated forest structure and composition include a) more accurate soil depth and soil carbon information, and b) incorporate cropland into the analysis. This study allowed for the presence of herbaceous plants within each ED2 tile, but did not explicitly define cropland from NLCD, which could affect the total sequestration potential of a pixel and region. At the scale of Massachusetts, recent state level data [43] estimated forest sequestration to 12% of the total state fossil fuel emissions between 2004-2008 (2.84 TgC yr^{-1} out of 23.15 TgC yr^{-1}). From this study, Massachusetts county level yearly sequestration ranged from 10-97% of emissions. Identifying county level emissions and sequestration over the US and other high emission countries could result in a devolved responsibility and action by local councils (e.g. see [44]).

ACKNOWLEDGMENT

This paper was supported by the Sussex Research Development Fund, project # 4290. The authors thank Pedram Rowhani for his support at the onset of this project.

REFERENCES

1. Le Quéré, C., *et al.* (2016). Global carbon budget 2016. *Earth Syst. Sci. Data Discuss.*, 8, 605–649.
2. UN-REDD (2015). UN REDD Programme Strategic Framework. 2016-2020.
3. Friedlingstein, P, *et al.* (2006). Climate–Carbon Cycle Feedback Analysis: Results from the C4MIP Model Intercomparison. *J. of Climate*, 19, 3337-3353.
4. Ahlström, A., *et al.* (2012). Robustness and uncertainty in terrestrial ecosystem carbon response to CMIP5 climate change projections. *Env. Res. Lett.*, 7, 044008.
5. Piao, S., *et al.* (2013). Evaluation of terrestrial carbon cycle models for their response to climate variability and to CO2 trends. *Glob. Change Biol., 19* (7), 2117-2132.
6. Næsset, E., *et al.* (2015). The effects of field plot size on model-assisted estimation of aboveground biomass change using multitemporal interferometric SAR and airborne laser scanning data. *Remote Sens. Environ.*, 168, 252-264.

7. Lu, D., *et al*. (2016). A survey of remote sensing-based aboveground biomass estimation methods in forest ecosystems. *Int. J. of Digit. Earth*, 9, 63-105.
8. Dubayah, R.O., Drake, J.B. (2000). Lidar remote sensing for forestry. *J. Forestry*, 98: 44-46.
9. Lefsky, M.A., *et al*. (2005). Estimates of forest canopy height and aboveground biomass using ICESat. *Geophys. Res. Lett.*, 32, L22S02.
10. Saatchi, S.S. et al. (2011). Benchmark map of forest carbon stocks in tropical regions across three continents. *PNAS*, 108, 9899–9904.
11. Baccini, A. *et al*. (2012). Estimated carbon dioxide emissions from tropical deforestation improved by carbon-density maps. *Nat. Clim. Change*, 2, 182-185.
12. Le Toan, T., *et al*. (2011). The BIOMASS mission: Mapping global forest biomass to better understand the terrestrial carbon cycle. *Remote sensing of environment*, 115 (11), 2850-2860.
13. Friedl, M.A. et al (2010). MODIS Collection 5 global land cover: Algorithm refinements and characterization of new datasets, *Remote Sens. Environ.*, 114, 168-182.
14. Homer, C.G., *et al*. (2015), Completion of the 2011 National Land Cover Database for the conterminous United States-Representing a decade of land cover change information. *Photogramm. Eng. Remote Sensing*, 81, 345-354.
15. Goodenough, D.G., *et al*. (2003). Processing hyperion and ali for forest classification. *IEEE Trans. Geosci. Remote Sens.*, 41, 1321–1331.
16. Roberts, D. A., *et al*. (1998). Mapping Chaparral in the Santa Monica Mountains using multiple endmember spectral mixture models. *Remote Sens. Environ.*, 65, 267-279.
17. Dennison, P.E., Roberts, D.A. (2003). Endmember Selection for Multiple Endmember Spectral Mixture Analysis using Endmember Average RSME, *Remote Sens. Environ.*, 87, 123-135.
18. Ranson, K. J., *et al*. (2001). Northern forest ecosystem dynamics using coupled models and remote sensing. *Remote Sens. Environ.*, 75, 291–302.
19. Kotchenova, S. Y., *et al*. (2004). Lidar remote sensing for modeling gross primary production of deciduous forests. *Remote Sens. Environ.*, 92, 158-172.
20. Chasmer, L., *et al*. (2011). Characterizing vegetation structural and topographic characteristics sampled by eddy covariance within two mature aspen stands using lidar and a flux footprint model: Scaling to MODIS. *J. Geophys. Res.: Biogeosci.*, 116.
21. Yang, W., *et al*. (2010): A clumped-foliage canopy radiative transfer model for a global dynamic terrestrial ecosystem model. II: Comparison to measurements. *Agr. Forest Meteorol.*, 150, 895-907.
22. Hurtt, G. C., *et al*. (2004). Beyond potential vegetation: combining Lidar data and a height-structured model for carbon studies. *Ecol. Appl.*, 14, 873-883.
23. Thomas, Q.R., *et al*. (2008). Using lidar data and a height-structured ecosystem model to estimate forest carbon stocks and fluxes over mountainous terrain, *Can. J. Remote Sens.*, 34, S351-S363.
24. Antonarakis, A.S., *et al*. (2011). Using Lidar and Radar measurements to constrain predictions of forest ecosystem structure and function. *Ecol. Appl.*, 21, 1120-1137.
25. Moorcroft, P.R., Hurtt, G. C., Pacala, S. W. (2001). A Method for Scaling Vegetation Dynamics: The Ecosystem Demography Model (ED). *Ecol. Monogr.*, 71 (4), 557-585.
26. Medvigy, D., *et al*. (2009). Mechanistic scaling of ecosystem function and dynamics in space and time: Ecosystem Demography model version 2. *J. Geophys. Res.: Biogeosci.*. 114, G01002.
27. Levine, N.M. *et al*. (2016). Ecosystem heterogeneity determines the ecological resilience of the Amazon to climate change. *PNAS*, 113 (3), 793-797.
28. Antonarakis, A.S., Munger, J.W., Moorcroft, P.R. (2014). Imaging Spectroscopy- and Lidar- derived Estimates of Canopy Composition and Structure Improve Predictions of Forest Carbon Fluxes and Ecosystem Dynamics, *Geophys. Res. Lett.*, 41 (7), 2535-2542
29. Zwally, H.J., *et al*. (2002). ICESat's laser measurements of polar ice, atmosphere, ocean, and land, *J. Geodyn.*, 34 (3-4), 405–445.
30. Brenner, A.C., *et al*. (2000). *Derivation of range and range distributions from laser pulse waveform analysis for surface elevations, roughness, slope, and vegetation heights. Algorithm theoretical basis document*. Version 3.0. Greenbelt, MD: Goddard Space Flight Center.
31. Hilbert, C. & Schmullius, C. (2012). Influence of Surface Topography on ICESat/GLAS Forest Height Estimation and Waveform Shape. *Remote Sensing*, 4, 2210-2235.
32. Ni-Meister, W., Jupp, D.L.B., Dubayah, R. (2001). Modeling Lidar Waveforms in Heterogeneous and Discrete Canopies. *IEEE Trans. Geosci. Remote Sens.*, 39, 1943-1958.
33. Ryu, Y., *et al*. (2010). On the correct estimation of effective leaf area index: Does it reveal information on clumping effects? *Agric. For. Meteorol.*, 150, 463-472.
34. Yang, W., *et al*. (2010). A clumped-foliage canopy radiative transfer model for a global dynamic terrestrial ecosystem model. II: Comparison to measurements. *Agr. Forest Meteorol*., 150, 895-907.
35. Breiman, L. (2001). Random forests. *Machine learning*, 45, 5–32.
36. Thornton, P.E., *et al*. (2016). *Daymet: Daily Surface Weather Data on a 1-km Grid for North America, Version 3*. ORNL DAAC, Oak Ridge, Tennessee, USA.
37. Mitchell, K.E., et al., (2004), The multi-institution North American Land Data Assimilation System (NLDAS): Utilizing multiple GCIP products and partners in a continental distributed hydrological modeling system. *J. Geophys. Res.: Atmos.*, 109, D07S90.
38. Rodríguez-Veiga, P., *et al*. (2016). Magnitude, spatial distribution and uncertainty of forest biomass stocks in Mexico. *Remote Sens. Environ.*, 183, 265-281.
39. Gurney, K.R., *et al*. (2009) The Vulcan Project: High resolution fossil fuel combustion CO_2 emissions fluxes for the United States, *Environ. Sci. Technol*, 43, 5535–5541.
40. USDA FS (2005) *FIA field manual version 3.0*. [online] Available https://www.fia.fs.fed.us/library/field-guides-methods-proc/docs/2006/p3_3-0_sec12_10_2005.pdf.
41. Riemann, R., *et al*. (2016). Comparative assessment of methods for estimating tree canopy cover across a rural-to-urban gradient in the mid-Atlantic region of the USA. *Environ. Monit. Assess.*, 188 (5), 1-17.
42. Treuhaft, R.N., *et al*. (2009). Vegetation profiles in tropical forests from multibaseline interferometric synthetic aperture radar, field, and lidar measurements. *J. Geophys. Res.: Atmos.*, 114, D23110.
43. Massachusetts EEA (2016). *Greenhouse Gas (GHG) Emissions in Massachusetts*. [online] Available http://www.mass.gov/eea/agencies/massdep/climate-energy/climate/ghg/greenhouse-gas-ghg-emissions-in-massachusetts.html.
44. United Kingdom Committee on Climate Change (2012). *How local authorities can reduce emissions and manage climate risk*. Policy Report.

Alexander S. Antonarakis received a BSc in geographic sciences in Bristol University, UK in 2004, and a PhD at Cambridge University in 2009.

From 2008-2013 he was a Postdoctoral Researcher at the department of organismic and evolutionary biology at Harvard University. Since 2013 he is a Lecturer of geography at the University of Sussex, UK. His research interests are on the interface of terrestrial ecology, climate change, and flooding in relation to forest ecosystems. He has made extensive use of remote sensing in his work including lidar, radar, multi and hyperspectral imagery.

Alejandro Guizar Coutiño received a BA in international affairs from the Universidad del Valle de México in 2008. He holds an MSc in Climate Change and Development from the University of Sussex, United Kingdom (2013). From late 2014 he has been collaborating with the Luc Hoffmann Institute as the Data Analytics expert. His research interests encompass climate change adaptation, sustainable development and biodiversity conservation.